Humanoid Robot Balance Control Using CoM Height Variations

B.J. van Hofslot

Master of Science Thesis

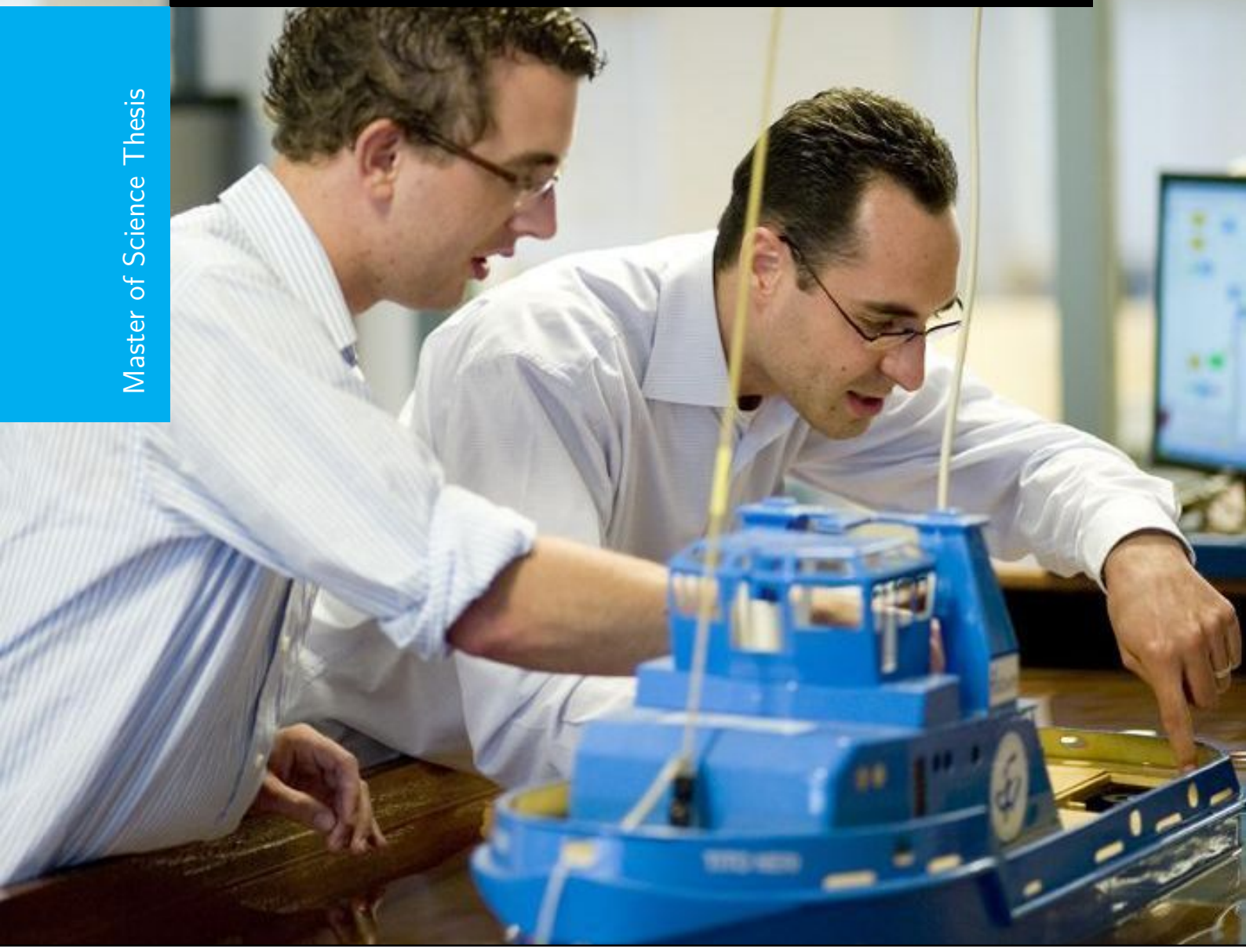

TU Delft Delft University of Technology

Cognitive Robotics

Humanoid Robot Balance Control Using CoM Height Variations

Master of Science Thesis

For the degree of Master of Science in Systems and Control at Delft University of Technology

B.J. van Hofslot

October 11, 2018

Faculty of Mechanical, Maritime and Materials Engineering (3mE) · Delft University of Technology

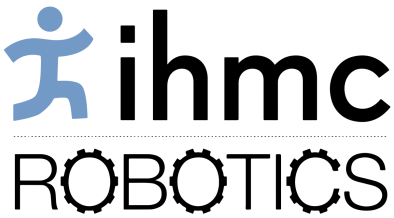

The work in this thesis was supported by the Institute for Human and Machine Cognition. Their cooperation is hereby gratefully acknowledged.

Abstract

This is an abstract.

Table of Contents

List of Figures

List of Tables

Preface

According to WikipediA, a preface (pronounced "*preffus*") is an introduction to a book written by the author of the book. In this preface I can discuss the interesting story of how this thesis came into being.

This is document is a part of my Master of Science graduation thesis. The idea of doing my thesis on this subject came after a discussion with my good friends Tweedledum and Tweedledee...

Acknowledgements

I would like to thank my supervisor prof.dr.ir. M.Y. First Reader for his assistance during the writing of this thesis...

By the way, it might make sense to combine the Preface and the Acknowledgements. This is just a matter of taste, of course.

Delft, University of Technology
October 11, 2018

B.J. van Hofslot

"Playing football is very simple, but playing simple football is the hardest thing there is."

— *Johan Cruyff*

Chapter 1

Introduction

1-1 Motivation

A common approach in humanoid robotics is to define the system as a linear inverted pendulum (LIP) with finite-sized foot and a mass with inertia. The ankle and the angular momentum about the center of mass (CoM) can be used as control inputs to generate horizontal forces on the CoM, often called "ankle" and "hip" strategies. Allowing for the vertical component of the ground reaction force (GRF) in the model to vary, and thus the height to vary, the horizontal components of the GRF change as well, compared to the LIP model. Different reasons to research varying CoM height:

- Improve behavior over rough-terrain
- Minimize energy consumption or mimic natural behavior
- Analyse the effects of height variation
- Extend control authority in horizontal direction by using height variations

1-2 Research Objective

In this thesis is focussed on the last two goals. Analyse the effects of height variation. Extend the control authority by using height variations.

1-3 Contributions

- Theoretic limits on capture: different limits on capture are derived, considering height variation.

- Orbital energy model predictive control (MPC): with the two-dimensional space (2D) method of [1] a constrained MPC is introduced.
- Approach for application on real robot: approaches are derived to implement in the control framework at IHMC.

1-4 Thesis Outline

Chapter 2

Background

2-1 Modeling of Walking

2-1-1 Simple Walking Model

Mass, inertia, finite-sized foot.

2-1-2 Linear Inverted Pendulum Model

In modeling of walking, one of the most important assumptions often made is the modeling of the stance leg as a linear inverted pendulum (LIP), as for example in [2]. Besides this, a not-linearized inverted pendulum is also widely used in the modeling of walking [3]. For planning and control however, a linearized description is desirable. In the two-dimensional space (2D) LIP equations of motion

$$\ddot{x} = \frac{g}{l}x \tag{2-1}$$

where l is the pendulum length and x the Cartesian x-coordinate of the pendulum tip, the motion of the tip along the x-axis does not affect l. At any position x, a local virtual straight pendulum can be considered, so this motion is at a constant height and $l = z_0$ holds. As in three-dimensional space (3D) by the linear model the system dynamics can be decoupled, the dynamics in y-direction read the same: $\ddot{y} = \frac{g}{l}y$. In Figure 2-1 this motion is visualized if the center of mass (CoM) is relatively far from from the base. The pendulum base lies in the origin and $\boldsymbol{x} = [x, y]^T$ is the 2D CoM projection on the horizontal plane. Because the LIP assumption holds, the vertical component of the leg force $\boldsymbol{f}$ has to cancel out gravity acceleration: $f_z = mg$.

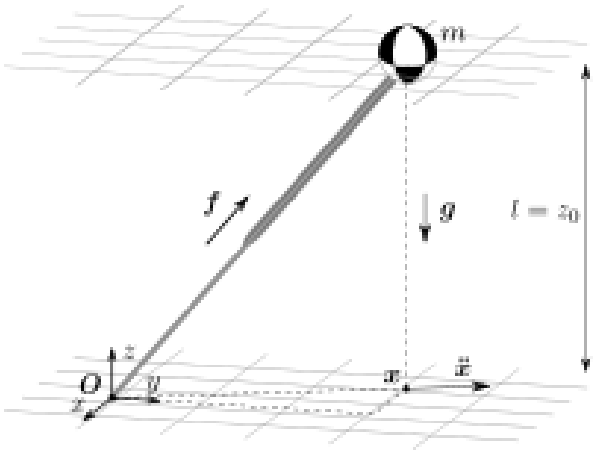

Figure 2-1: 3D motion of LIP model.

2-1-3 Nonlinear Models

2-2 Measured Quantities & Ground Reference Points in Walking

2-2-1 Ground Reaction Force

A common approach for quantifying the dynamics of a walker, either a human or a robot, is the use of a ground reaction force (GRF), coming a from a single point of application on the ground. The magnitude and direction of the force vector, the gravitational vector, other external forces and the robots state determine the dynamics of the system.

2-2-2 The center of pressure (CoP)

The feet attached to the LIP robot model increase the possibilities to control its motion. The ankles can apply a torque that would virtually move the position of the base of the inverted pendulum, so that the linear acceleration on the CoM as in Eq. (2-1) and the capture point as in Eq. (2-7) change. The new virtual base is called the CoP. By its definition, this point only lives within the support polygon [4]. In Figure 2-2 the definition of the CoP is visualized. If the point mass is restricted to move on a constant height, the vertical component of $\boldsymbol{f'}$ counteracts gravity: $f'_z = g$.

2-2-3 The zero moment point (ZMP)

The ZMP coincides during stable walking with the CoP, like described in [4]. The two points however are not equal in unstable or more complicated cases, like falling over. The CoP is restricted to be in the support polygon, as this is a point that links to contact forces [5]. The ZMP however is not restricted to lie within the support polygon. The ZMP is the point on the ground where the tipping moment equals zero. The tipping moment is defined as the component of the moment that is tangential to the ground surface. The ZMP initially was introduced in [6].

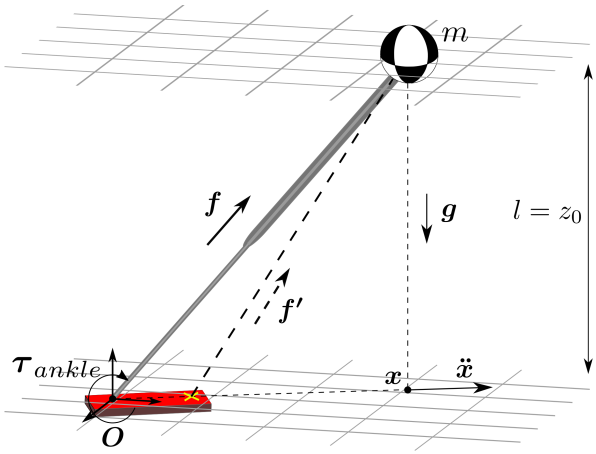

Figure 2-2: 3D motion of LIP model with foot. The yellow cross points out the CoP location.

2-2-4 The centroidal momentum pivot (CMP)

The earlier mentioned points give sufficient measure for a LIP model with point mass and finite-sized feet. However, any angular momentum applied by the body does not affect those points. In the case of the CoP for example, the model assumes the resulting reaction force acts from the CoP through the CoM. The CMP takes angular momentum into account, which can be used as a measure and for control [7]. This is defined as the point where a line passing through the CoM, parallel to the ground reaction force intersects with the ground surface. The CMP is defined as

$$x_{CMP} = x_{ZMP} + \frac{\tau_{y,CoM}}{F_{gr,z}} \tag{2-2}$$

$$y_{CMP} = y_{ZMP} - \frac{\tau_{x,CoM}}{F_{gr,z}} \tag{2-3}$$

where τ_{CoM} is the torque around the CoM, $[x_{ZMP}, y_{ZMP}]$ the ZMP location on the horizontal plane and $F_{gr,z}$ is the ground reaction force in z-direction in Cartesian space. In Figure 2-3 is displayed how body angular momentum affects the ground reaction force $\boldsymbol{f'}$ from the CoP and how the CMP can be determined with the intersection of a parallel line through the CoM and the ground plane. For clarity the point in the image lies on the line from $\boldsymbol{O}$ to $\boldsymbol{x}$. This has not to be the case however, as the body can exert angular momentum along all axes.

2-2-5 Other Points

2-3 Energy of Walking

2-3-1 LIP Orbital Energy

A crucial finding in an extended use of LIP models can be found in [8]. Because force is mass times acceleration: $F = ma$, impuse momentum is force times velocity: $I = Fv$ and the energy or work done by a force is the force times the distance, and thus the impulse integrated

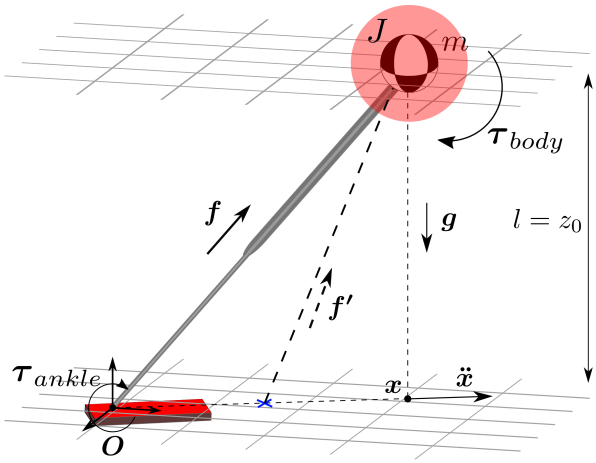

Figure 2-3: 3D motion of LIP model with foot and body inertia. The blue cross points out the CMP location.

over the time interval: $E = Fs = \int Fvdt$, there can be reasoned that if one takes the time integral of the product of the second and the first derivative of a state, an expression for a normalized energy can be achieved: $\frac{E}{m} = \int avdt$. In the mentioned publication that same action is applied on Eq. (2-1):

$$\int (\ddot{x} - \frac{g}{l}x)\dot{x}dt = \frac{1}{2}\dot{x}^2 - \frac{g}{2z_0}x + C = 0 \tag{2-4}$$

with C the integration constant. The LIP Orbital Energy is defined as $E_{LIP} = -C$. If $E_{LIP} > 0$, the point mass will cross the x position of the pendulum base with its current velocity. If $E_{LIP} < 0$, the point mass will not cross the pendulum base and will have a turning point where the velocity becomes zero.

The instantaneous capture point (ICP)

Although the finding of the LIP Orbital Energy was very important for future robot motion modeling, more than a decade later [9] introduced the capture point (CP). Taking $E_{LIP} = 0$ and taking the square root of Eq. (2-4) gives

$$x_{CP} = \sqrt{\frac{z_0}{g}}\dot{x} \tag{2-5}$$

where x_{CP} is the CP, measured from the current pendulum tip position, based on the current tip velocity $\dot{x}$. This is the point where the velocity is exactly driven to zero and the pendulum is upright, where neither crossing of the pendulum base ocurred nor turning of body velocity. In Figure 2-4 a 2D visual explanation is given of this point. Later, the ICP was introduced [10], which gives a slightly different discription of the point:

$$x_{ICP} = x + \sqrt{\frac{z_0}{g}}\dot{x} \tag{2-6}$$

where x_{ICP} is the ICP. In this way, the point can be described in the environment coordinates. The x- and y-coordinate can be decoupled as in the equations of motion of Eq. (2-1). However,

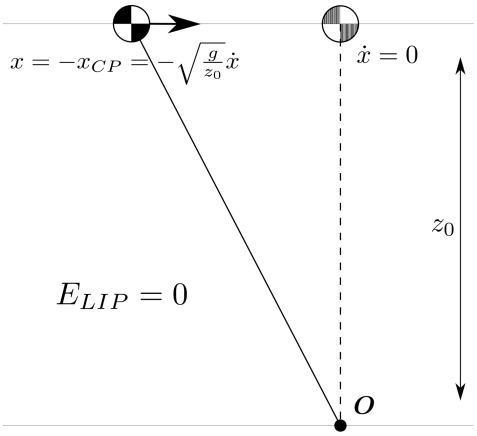

Figure 2-4: Visualization of path and states by the capture of the point mass according ICP theory.

in the 2D horizontal plane, convergence to the capture point in one direction does not include convergence to the capture point in the other. In other words: the direction of motion is not restricted to move towards the pendulum base as in the sideview case.

ICP dynamics

Because the ankle is not always located at the same location as the ICP for the current horizontal velocity, for modeling and planning the time derivative is taken of the ICP, which is named the ICP dynamics [10]. This time derivative can be written as a function of the current ICP location:

$$\dot{\boldsymbol{x}}_{ICP} = \sqrt{\frac{g}{z_0}}\boldsymbol{x}_{ICP} \tag{2-7}$$

where $\boldsymbol{x}_{ICP}$ is the xy-vector of the ICP location and assuming that the pendulum base is the origin.

2-3-2 Nonlinear Orbital Energy

Writing the nonlinear trajectory of a 2D model as $z = f(x)$, a similar expression of energy as $E_{LIP}$is derived in [11]

$$E_{orbit} = \frac{1}{2}\dot{x}^2\bar{f}^2(x) + gx^2 f(x) - 3g\int_{x_0}^{x} f(\xi)\xi d\xi = \frac{1}{2}\dot{x}_0^2\bar{f}^2(x_0) + gx_0^2 f(x_0). \tag{2-8}$$

E_{orbit}

2-3-3 Boundedness Condition

In [12]:

$$x_u(t,z) = e^{\omega_0(t-t_0)}x_u(t_0) - \omega_0\int_{t_0}^{t} e^{\omega_0(t-\tau)}r(\tau)d\tau \tag{2-9}$$

bounded if:

$$x_u(t_0) = \omega_0 \int_{t_0}^{\infty} e^{-\omega_0(\tau - t_0)} r(\tau) d\tau \tag{2-10}$$

This is extended in an varying height expression in...

2-4 Related Works CoM Height Variation

2-4-1 Varying Height Terrain

A lot of publications that incorporate the height variations in the terrain in the dynamic planning problem. [13] [14] and more..

2-4-2 Mimic Natural Behavior

Straight leg walking. [15] and more..

2-4-3 Effects of Height Variation

Research that investigates the energetic influences of height variations and impacts, often human orientated. [3] [16] [17] and more..

2-4-4 Control for Balance

Two publications that consider height variations as control input for balance: [1] [18] This is the focus in this thesis.

2-5 Humanoid Robotics at IHMC

2-5-1 Robots

Atlas, Valkyrie.

2-5-2 Walking States

- single support (SS)
- double support (DS)
- Toe-Off

2-5-3 Planning

Footstep Planning

User defined in graphical user interface (GUI) or A* planner. Terrain information given by perception data (LiDAR).

ICP Planning

ICP planning is the creation of a dynamical plan based on predefined footstep locations, the desired step time and the LIP model of the system . Earlier approaches consider one CoP knotpoint per footstep and integrate the ICP dynamics backwards in time from the last footstep, considering the knotpoints to remain constant. Current improvements include double support, heel-toe multiple knotpoints, angular momentum prediction, continous CMP trajectories instead of knotpoints.

2-5-4 ICP Control

From an CMP and ICP reference trajectory, the following control law is used to generate a desired CMP:

$$\mathbf{r}_{cmp,d} = \mathbf{r}_{cmp,r} + \mathbf{k}_\xi(\xi - \xi_r). \tag{2-11}$$

From the desired CMP, a desired horizontal linear momentum rate of change, a desired horizontal force, can be determined:

$$\dot{\mathbf{l}}_{d,xy} = \frac{\mathbf{c}_{xy} - \mathbf{r}_{cmp,d}}{z_0} mg. \tag{2-12}$$

The desired horizontal linear momentum rate of change $\dot{\mathbf{l}}_{d,xy}$ is an input for the momentum-based controller.

2-5-5 Momentum-based Control & Inverse Dynamics

Dynamics humanoid

- End-effector motion: $\boldsymbol{T} = \begin{bmatrix} \boldsymbol{\omega} \\ \boldsymbol{v} \end{bmatrix} = \boldsymbol{J}(\boldsymbol{q})\dot{\boldsymbol{q}}$, Jacobian maps joint velocities to endeffector twist, or sometimes to other joint velocities.
- Centroidal momentum: $\boldsymbol{h} = \begin{bmatrix} \boldsymbol{k} \\ \boldsymbol{l} \end{bmatrix} = \boldsymbol{A}(\boldsymbol{q})\dot{\boldsymbol{q}}$, $\boldsymbol{A} = \boldsymbol{I}\boldsymbol{J}$ (Inertia * Jacobian)
- Dynamics: $\dot{\boldsymbol{h}} = \begin{bmatrix} \dot{\boldsymbol{k}} \\ \dot{\boldsymbol{l}} \end{bmatrix} = \boldsymbol{A}\ddot{\boldsymbol{q}} + \dot{\boldsymbol{A}}\dot{\boldsymbol{q}} = \boldsymbol{W}_g + \sum_i \boldsymbol{W}_{gr,i} + \sum_i \boldsymbol{W}_{ext,i}$, rate of change of centroidal momentum depends on external wrenches.
- Ground reaction wrench: $\sum_i \boldsymbol{W}_{gr,i} = \boldsymbol{Q}\boldsymbol{\rho}$, (contact matrix * basis vector multipliers). Wrench cone.

Whole-body QP

The desired vertical linear momentum rate is computed with the control loop

$$\dot{\boldsymbol{l}}_z = m(k_p(z - z_r) + k_d\dot{z}) \tag{2-13}$$

with bounds on resulting $\dot{z}$ and $\ddot{z}$.
QP: Find desired joint accelerations and ground reaction forces based on objectives. The objectives consist of a momentum objective, motion objectives, regularization terms and a null-space projection objective. The desired momentum is only determined by the desired linear momentum rate of change, the angular part is left unconstrained. An estimate of the amount of angular momentum rate of change that is needed to fulfill the desired linear momentum rate of change objective is given by the distance of the desired CMP outside the foot polygon. If the CMP is inside the foot polygon no angular momentum is needed, 'ankle' strategies are enough to fulfill the desired linear momentum rate. Motion tasks include: desired foot trajectories, desired body orientation, desired spine joint position. Desired motion comes from PD-control. The null-space projection term can be used to input privileged joint accelerations, when the null-space of an robotic chain opens up, to avoid singularity.
The motion tasks and momentum tasks can conflict and the solution is always a trade-off, depending on the weights.

$$\begin{aligned} \min_{\ddot{\boldsymbol{q}}_d, \boldsymbol{\rho}} \quad & J_{\dot{\boldsymbol{h}}_d} + J_{\boldsymbol{J}} + J_{\boldsymbol{\rho}} + J_{\ddot{\boldsymbol{q}}_d} + J_p \\ \text{s.t.} \quad & \boldsymbol{A}\ddot{\boldsymbol{q}}_d + \dot{\boldsymbol{A}}\dot{\boldsymbol{q}} = \boldsymbol{W}_g + \boldsymbol{Q}\boldsymbol{\rho} + \textstyle\sum_i \boldsymbol{W}_{ext,i} \\ & \boldsymbol{\rho}_{min} \leq \boldsymbol{\rho} \\ & \ddot{\boldsymbol{q}}_{min} \leq \ddot{\boldsymbol{q}}_d \leq \ddot{\boldsymbol{q}}_{max} \end{aligned}$$

$$\begin{aligned} \text{Momentum objective:} \quad & J_{\dot{\boldsymbol{h}}_d} = \boldsymbol{R}_{\dot{\boldsymbol{h}}_d}||(\boldsymbol{A}\ddot{\boldsymbol{q}}_d - \boldsymbol{b}||^2 \\ \text{Motion objective:} \quad & J_{\boldsymbol{J}} = \boldsymbol{R}_{\boldsymbol{J}}||(\boldsymbol{J}\ddot{\boldsymbol{q}}_d - \boldsymbol{p})||^2 \\ \text{Contact force cost:} \quad & J_{\boldsymbol{\rho}} = \boldsymbol{R}_{\boldsymbol{\rho}}||\boldsymbol{\rho}||^2 \\ \text{Joint acceleration cost:} \quad & J_{\ddot{\boldsymbol{q}}_d} = \boldsymbol{R}_{\ddot{\boldsymbol{q}}_d}||\ddot{\boldsymbol{q}}_d||^2 \\ \text{Privileged configuration:} \quad & J_p = \boldsymbol{R}_p||(\boldsymbol{I} - \boldsymbol{J}_t^{\dagger}\boldsymbol{J}_t)\ddot{\boldsymbol{q}}_p - \ddot{\boldsymbol{q}}_d||^2 \end{aligned}$$

- $\boldsymbol{b} = \dot{\boldsymbol{h}}_d - \dot{\boldsymbol{A}}\dot{\boldsymbol{q}}$, only linear momentum rate of change selected as objective: $\boldsymbol{S}\dot{\boldsymbol{h}}_d = \dot{\boldsymbol{l}}_d$
- $\boldsymbol{p} = \dot{\boldsymbol{T}} - \dot{\boldsymbol{J}}\dot{\boldsymbol{q}}$, (in case of end effector motion)
- $\boldsymbol{J} = [\boldsymbol{J}_1^T \quad ... \quad \boldsymbol{J}_N^T]^T$, concatenated Jacobians of motion tasks
- $\boldsymbol{J}_t = [(\boldsymbol{S}\boldsymbol{A})^T \quad \boldsymbol{J}^T]^T$, big Jacobian for all tasks
- $(\boldsymbol{I} - \boldsymbol{J}_t^{\dagger}\boldsymbol{J}_t)$, null-space projector in case of a *redundant* system (*overdetermined*: joints have more degrees of freedom than end-effector motion)
- $\boldsymbol{J}^{\dagger} = \boldsymbol{J}^T(\boldsymbol{J}\boldsymbol{J}^T + \mu^2)^{-1}$, Moore-Penrose left (damped) pseudoinverse. $\mu > 0$: damping factor.

Inverse Dynamics

Desired joint torques $\boldsymbol{\tau}_d$ are calculated via inverse dynamics using solution of QP: $\ddot{\boldsymbol{q}}_d$ and $\boldsymbol{\rho}$.

- $\boldsymbol{\tau}_d = \boldsymbol{M}(\boldsymbol{q})\ddot{\boldsymbol{q}}_d + \boldsymbol{C}(\boldsymbol{q}, \dot{\boldsymbol{q}}) + \boldsymbol{G}(\boldsymbol{q}) + \boldsymbol{J}^T\boldsymbol{f}$, where $\boldsymbol{f}$ is the linear part of the ground reaction wrench.

Chapter 3

Theoretic Limits on Capture

In this chapter there is looked at the point foot - point mass model, so no angular momentum is included.
This chapter matches the goal of exploring the effects of height variation.
A common habit is to formulate an optimization problem, and to 'let the optimization figure it out', but there is not looked at limits.
In the point-foot, point-mass model with prismatic leg joint, the constraints are:

- Unilateral ground reaction force
- Limit on leg length
- Limit on leg force
- Limit on ground friction

3-1 Unconstrained Capture Region

In this section the bounds are given with respect to capturability of a horizontal traveling CoM, like with the study of the capture point. The only constraint taken into account is unilaterality of ground reaction force (GRF). Also a measure of this limit is given in terms of the CP.
Balistic touchdown time for a given height is:

$$t = \sqrt{\frac{2z_0}{g}} \tag{3-1}$$

The horizontal location is:

$$x_{balistic} = \dot{x}t = \dot{x}\sqrt{\frac{2z_0}{g}} \tag{3-2}$$

which is then compares to the capture point as:

$$x_{balistic} = \sqrt{2}x_{cp} \tag{3-3}$$

This can also be reasoned from a leg force perspective, as no energy is substracted from the CoM during its travel.
Using this formulation of the problem and E_{LIP}:

$$x^2_{balistic} = \frac{z_0}{g}(\dot{x}_0^2 + \dot{x}_f^2) \tag{3-4}$$

Capture limits: leg can apply an infinite force just after the current position to stop on that horizontal location. The other side of the bound is the balistic touch down point, where the virtual leg can apply an impact when the mass hits the ground equal to its velocity and in the direction, then lift the mass up to the desired or default height. This limit on the capture region is defined as:

$$\{x_{cp} \in (0, \dot{x}\sqrt{\frac{2z_0}{g}}]\} \tag{3-5}$$

[1] Figure 3-1

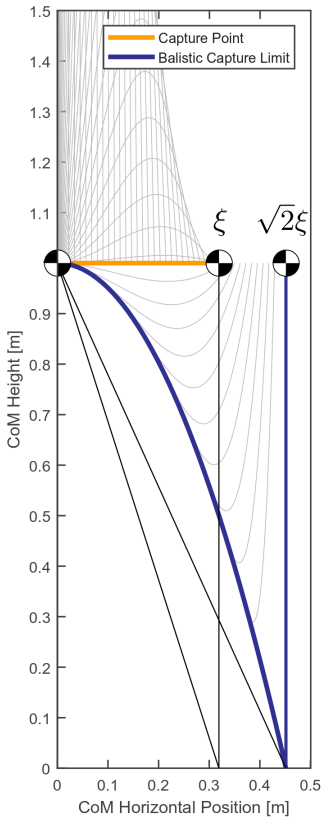

Figure 3-1: Unconstrained capture region and balistic limit, grey plots visualize intermediate trajectories and are made with the method of [1]

3-2 Height Constrained Capture

No leg length constriant, but height constraint. Figure 3-2

$$x_{cp,height} = (\frac{\sqrt{2g\delta z_{max}}}{g} + \sqrt{\frac{z_o + \delta z_{max}}{g}})(\dot{x}_0 - \frac{x_0}{z_0}\sqrt{2g\delta z_{max}}). \tag{3-6}$$

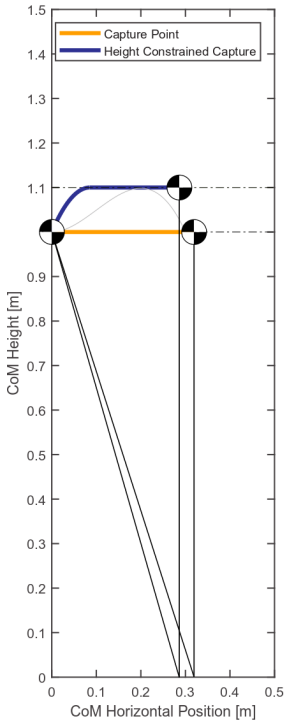

Figure 3-2: Height constrained capture limit. Grey plot is made with the method of [1] and shows that the final point lies between the limit and the capture point (CP)

3-3 Impact Influenced Capture

$$x_{cp,impact} = \sqrt{\frac{z}{g}}(\dot{x} + \dot{x}_I) \tag{3-7}$$

$$x_{cp,impact} = \sqrt{\frac{z}{g}}(\dot{x} + \frac{x}{z}\dot{z}) \tag{3-8}$$

$$x_{cp,impact} = \frac{z}{\sqrt{zg} - \dot{z}} \tag{3-9}$$

[3], mention also straight leg walking, planning.

Chapter 4

Orbital Energy MPC

This model predictive control (MPC) method is based on the method of [1], which relies on E_{orbit} derived in [11]

4-1 2D Polynomial

Added a final velocity term $\dot{x_f}$ to the method of [1].

$$\frac{1}{2}\dot{x}^2\bar{f}^2(x) + gx^2 f(x) - 3g\int_{x_0}^{x} f(\xi)\xi d\xi = \frac{1}{2}\dot{x}_0^2\bar{f}^2(x_0) + gx_0^2 f(x_0). \tag{4-1}$$

$$u = \frac{g + f''(x)\dot{x}^2}{\bar{f}(x)} \tag{4-2}$$

$$\underbrace{\begin{bmatrix} 1 & 0 & 0 & 0 \\ 1 & x_0 & x_0^2 & x_0^3 \\ 0 & 1 & 2x_0 & 3x_0^2 \\ \frac{3}{2}gx_0^2 & gx_0^3 & \frac{3}{4}gx_0^4 & \frac{3}{5}gx_0^5 \end{bmatrix}}_{A} \underbrace{\begin{bmatrix} c_0 \\ c_1 \\ c_2 \\ c_3 \end{bmatrix}}_{\boldsymbol{c}} = \underbrace{\begin{bmatrix} z_f \\ z_0 \\ \frac{\dot{z}_0}{\dot{x}_0} \\ k \end{bmatrix}}_{\boldsymbol{b}} \tag{4-3}$$

where $k = \frac{1}{2}(\dot{x}_0 z_0 - \dot{x}_0 x_0)^2 + gx_0^2 z_0 - \frac{1}{2}z_f^2\dot{x}_f^2$.

Changing $\dot{x_f}$, changes the trajectory, which can be used in optimization.

4-1-1 Height Constraint

Maximum height. Algorithm 1.

Algorithm 1 Find cubic polynomial constants under height constraint

procedure FINDPOLZ($A^{-1}, \boldsymbol{b}(\dot{x}_f)$)
  $\dot{x}_f \leftarrow 0$ ▷ Initial guess
  repeat
    $\boldsymbol{c} \leftarrow A^{-1}\boldsymbol{b}(\dot{x}_f)$ ▷ Find polynomial constants
    $x_{zmax} \leftarrow \frac{-2c_2+\sqrt{4c_2^2-12c_3c_1}}{6c_3}$ ▷ Traj. peak lies on highest x
    $z_{max} \leftarrow c_0 + c_1x_{zmax}^2 + c_2x_{zmax}^3 + c_3x_{zmax}^3$ ▷ Corresponding height
    $\dot{x}_f \leftarrow \dot{x}_f + \alpha$ ▷ Some smart increment
  until $z_{max} < z_{const}$
return $\boldsymbol{c}$
end procedure

4-1-2 Leg Length Constraint

Algorithm 2

$$(\sum_{n=0}^{3} c_n x^n)^2 = \sum_{n=0}^{3} c_n^2 x^{2n} + \sum_{\substack{n=1 \\ i+j=n \\ i<j}}^{3} c_i c_j x^n \tag{4-4}$$

Algorithm 2 Find cubic polynomial constants under leg length constraint

procedure FINDPOLL($A^{-1}, \boldsymbol{b}(\dot{x}_f)$)
  $\dot{x}_f \leftarrow 0$ ▷ Initial guess
  repeat
    $\boldsymbol{c} \leftarrow A^{-1}\boldsymbol{b}(\dot{x}_f)$ ▷ Find polynomial constants
    $x_{lmax}^2 \leftarrow \frac{-4c_2^2+\sqrt{16c_2^4-24c_3^2(2+2c_1^2)}}{12c_3^2}$ ▷ $d(f(x)^2+x^2)/dx = 0$
    $x_{lmax} \leftarrow -|\sqrt{x_{l^2max}}|$ ▷ Complex solutions
    $l_{max}^2 \leftarrow x_{lmax}^2 + (c_0 + c_1x_{zmax}^2 + c_2x_{zmax}^3 + c_3x_{zmax}^3)^2$
    $\dot{x}_f \leftarrow \dot{x}_f + \alpha$ ▷ Some smart increment
  until $l_{max}^2 < l_{const}^2$
return $\boldsymbol{c}$
end procedure

4-1-3 Challenges 3D Orbital Energy

4-2 Results

A planar walker that recovers from a push, where conventional center of pressure (CoP) control does not let it recover.

4-3 Discussion

2D..

Chapter 5

Towards Application

5-1 Challenges

5-1-1 Angular Momentum and Height Variation

Normal control framework IHMC:

$$F_x = \frac{x - x_{cmp,d}}{z_0} mg. \tag{5-1}$$

So scaling up F_x with F_z could be an option. Formulas center of pressure (CoP) and centroidal momentum pivot (CMP):

$$x_{cop} = x - \frac{F_x}{F_z} - \frac{\tau_y}{F_z} \tag{5-2}$$

$$x_{cmp} = x - \frac{F_x}{F_z} \tag{5-3}$$

Special case where center of mass (CoM) is above CoP:

$$x - x_{cop} = 0 \tag{5-4}$$

$$\frac{F_x}{F_z} + \frac{\tau_y}{F_z} = 0. \tag{5-5}$$

Im this situation, scaling up F_x with F_z, τ_y only contributes to F_x. So for contribution of added F_z, look at CoP:

$$F_x = \frac{x - x_{cop}}{z} F_z - \frac{\tau_y}{z} \tag{5-6}$$

The effects of changing the ground reaction compared to the CMP and not with the CoP are visualized in Figure 5-1

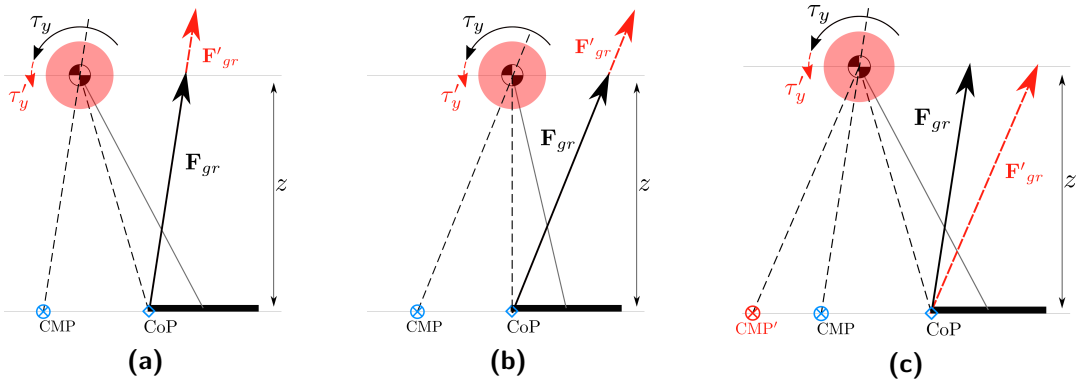

Figure 5-1: Effects of change in ground reaction force on angular momentum around the CoM. (a) F_x can be scaled up with F_z, which results in an increase in τ_y. (b) Situation where additional F_z does not contribute to additional F_x. (c) With a shifted CMP, a larger F_x can be achieved than with the strategy in (a).

5-1-2 From 2D to 3D

Direction of desired force can be out of plane with virtual leg between CoM and CoP. Only one input, F_z, can be used to control errors in two directions: x and y. If the direction of the desired force is orthogonal to the virtual leg, F_z has no effect. If F_z is increased in one direction, the unstable eigenvalue of the system in the other direction grows.

5-1-3 Leg Reachability

Stance leg and swing leg singularity need to be avoided. Also, to let the swing leg touch down at the desired time, the ground must be reachable at that time instance.

5-1-4 Predictability of Dynamics

Considering the current error, is the motion recoverable considering the constraints?

5-2 Experimental Setup

Atlas or Valkyrie walking over a terrain with limited foot placement options, so step adjustment is not possible (tiled environment). Push recovery to test disturbance rejection. See Table 5-1 for the used parameters.

5-3 Methods

Other publications that consider CoM height variations for balance use model predictive control (MPC). Considering worst-case scenario's, where additional horizontal force is needed, 'the best you can do' is needed to not fall over. This motivates to use a proportional controller in worst case scenario's, next to the benefit of simplicity and robustness.

Table 5-1: Stepping Parameters

Parameter	Value	Unit
Step Legth	0.5	[m]
Step Width	0.25	[m]
SS Time	0.6	[s]
DS Time	0.15	[s]

5-3-1 Quadratic Program Setup

One method: use lower weight on vertical momentum rate. To avoid singularity, a feedback based on a virtual spring, priviliged joint accelerations can be projected in the null-space.

5-3-2 Quadratic Program Inputs

Control Architecture

To actively change the desired momentum rate, the effects of additional height acceleration is included in the control framework as follows. Horizontal linear momentum rate formula in terms of CMP:

$$\dot{\mathbf{l}}_d = \frac{\mathbf{c}_{xy} - \mathbf{r}_{cmp,d}}{z} F_z \tag{5-7}$$

Horizontal linear momentum rate formula in terms of CoP:

$$\dot{\mathbf{l}}_d = \frac{\mathbf{c}_{xy} - (\mathbf{r}_{cop,d} + \frac{\tau_y}{F_z})}{z} F_z \tag{5-8}$$

$$\dot{\mathbf{l}}_d = \frac{\mathbf{c}_{xy} - \mathbf{r}_{cop,d}}{z} m(g + \ddot{z}_d) - \frac{\tau_y}{z} \tag{5-9}$$

This can be written as:

$$\dot{\mathbf{l}}_d = \underbrace{\frac{\mathbf{c}_{xy} - \mathbf{r}_{cmp,d}}{z} mg}_{\dot{\mathbf{l}}_{d,lip}} + \underbrace{\frac{\mathbf{c}_{xy} - \mathbf{r}_{cop,d}}{z} m\ddot{z}_d}_{\dot{\mathbf{l}}_{d,heightcontrol}}, \tag{5-10}$$

where $\dot{\mathbf{l}}_{d,lip}$ is the standard desired horizontal momentum rate term and $\dot{\mathbf{l}}_{d,heightcontrol}$ is the additional momentum rate from height control.

Control Strategy

If the following criteria are met:

1. the desired CMP is a certain distance outside the foot polygon
2. a height or singularity constraint is not met
3. the angle between the ICP error and the virtual leg between CoP and CoM in the xy transverse plane is not larger than a specifice value.

ramp up the desired height acceleration with a constant maximum jerk, until the maximum acceleration is reached. Then hold this maximum acceleration, until one of the criteria does not hold anymore.
As the strategy is only used when the CMP is outside the foot polygon, an estimate of the resulting CoP is made by projecting the desired CMP on the foot polygon.
Figure 5-3 shows initial and final CoM and instantaneous capture point (ICP) configurations for single support (SS). Figure 5-4 shows different alignment angles for the initial configuration, when entering SS.
Figure 5-2 shows an example of a resulting control profile.

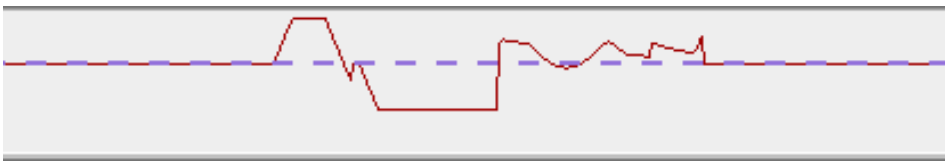

Figure 5-2: Resulting control profile after a push at start of SS

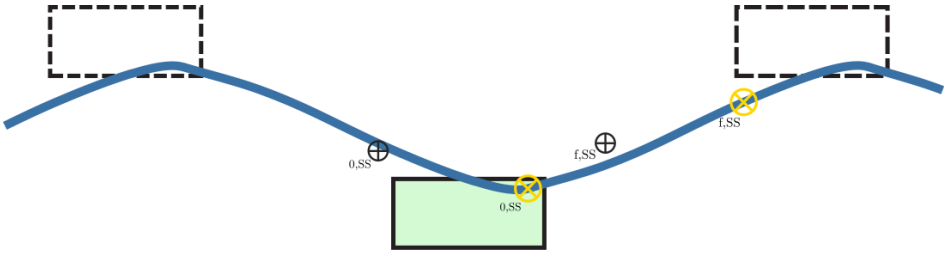

Figure 5-3: Initial (0,SS) and final (f,SS) configurations of CoM position (black circle with cross) and ICP reference (yellow circle with rotated cross) for SS in the xy-plane with the parameters from Table Table 5-1. The green area is the current supporting foothold and the blue line is the ICP reference trajectory.

5-4 Results

5-4-1 Simulation

Comparison with 'normal' control setup. (and comparison with 'ankle' and 'hip' strategies)

5-4-2 Hardware

5-5 Discussion

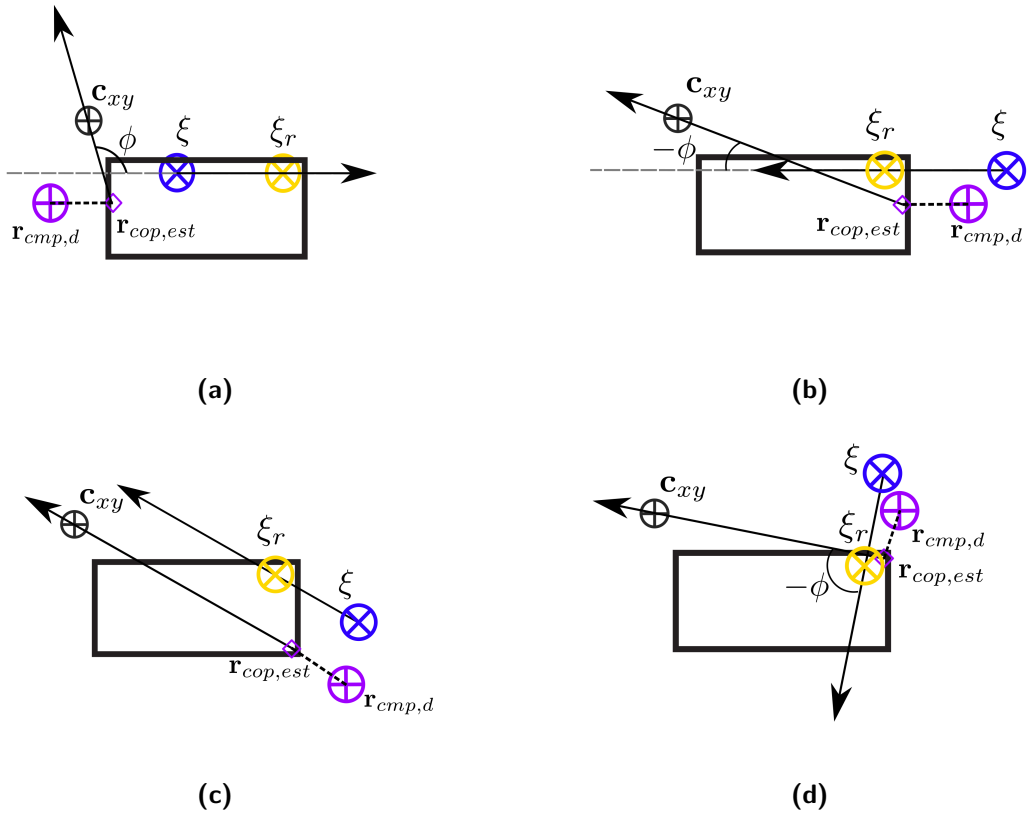

Figure 5-4: Vizualizations of the error alignment angle for the configuration at start of SS, with ICP errors: (a) negative in sagital plane, (b) positive in sagital plane, (c) where the error alignment angle is 0 and (d) where the error alignment angle is orthogonal to the ICP error.

Chapter 6

Conclusion

6-1 Recommendations

Bibliography

[1] T. Koolen, M. Posa, and R. Tedrake, "Balance control using center of mass height variation: limitations imposed by unilateral contact," in *Humanoid Robots (Humanoids), 2016 IEEE-RAS 16th International Conference on*, pp. 8–15, IEEE, 2016.

[2] S. Kajita, F. Kanehiro, K. Kaneko, K. Yokoi, and H. Hirukawa, "The 3d linear inverted pendulum mode: A simple modeling for a biped walking pattern generation," in *Intelligent Robots and Systems, 2001. Proceedings. 2001 IEEE/RSJ International Conference on*, vol. 1, pp. 239–246, IEEE, 2001.

[3] A. D. Kuo, J. M. Donelan, and A. Ruina, "Energetic consequences of walking like an inverted pendulum: step-to-step transitions," *Exercise and sport sciences reviews*, vol. 33, no. 2, pp. 88–97, 2005.

[4] M. Vukobratović and B. Borovac, "Zero-moment point—thirty five years of its life," *International journal of humanoid robotics*, vol. 1, no. 01, pp. 157–173, 2004.

[5] P. Sardain and G. Bessonnet, "Forces acting on a biped robot. center of pressure-zero moment point," *IEEE Transactions on Systems, Man, and Cybernetics-Part A: Systems and Humans*, vol. 34, no. 5, pp. 630–637, 2004.

[6] M. Vukobratovic and D. Juricic, "Contribution to the synthesis of biped gait," *IEEE Transactions on Biomedical Engineering*, no. 1, pp. 1–6, 1969.

[7] M. B. Popovic, A. Goswami, and H. Herr, "Ground reference points in legged locomotion: Definitions, biological trajectories and control implications," *The International Journal of Robotics Research*, vol. 24, no. 12, pp. 1013–1032, 2005.

[8] S. Kajita, T. Yamaura, and A. Kobayashi, "Dynamic walking control of a biped robot along a potential energy conserving orbit," *IEEE Transactions on robotics and automation*, vol. 8, no. 4, pp. 431–438, 1992.

[9] J. Pratt, J. Carff, S. Drakunov, and A. Goswami, "Capture point: A step toward humanoid push recovery," in *Humanoid Robots, 2006 6th IEEE-RAS International Conference on*, pp. 200–207, IEEE, 2006.

[10] T. Koolen, T. De Boer, J. Rebula, A. Goswami, and J. Pratt, "Capturability-based analysis and control of legged locomotion, part 1: Theory and application to three simple gait models," *The International Journal of Robotics Research*, vol. 31, no. 9, pp. 1094–1113, 2012.

[11] J. E. Pratt and S. V. Drakunov, "Derivation and application of a conserved orbital energy for the inverted pendulum bipedal walking model," in *Robotics and Automation, 2007 IEEE International Conference on*, pp. 4653–4660, IEEE, 2007.

[12] L. Lanari, S. Hutchinson, and L. Marchionni, "Boundedness issues in planning of locomotion trajectories for biped robots," in *Humanoid Robots (Humanoids), 2014 14th IEEE-RAS International Conference on*, pp. 951–958, IEEE, 2014.

[13] J. Englsberger, C. Ott, and A. Albu-Schäffer, "Three-dimensional bipedal walking control using divergent component of motion," in *Intelligent Robots and Systems (IROS), 2013 IEEE/RSJ International Conference on*, pp. 2600–2607, IEEE, 2013.

[14] M. A. Hopkins, D. W. Hong, and A. Leonessa, "Humanoid locomotion on uneven terrain using the time-varying divergent component of motion," in *Humanoid Robots (Humanoids), 2014 14th IEEE-RAS International Conference on*, pp. 266–272, IEEE, 2014.

[15] R. J. Griffin, G. Wiedebach, S. Bertrand, A. Leonessa, and J. Pratt, "Straight-leg walking through underconstrained whole-body control," in *2018 IEEE International Conference on Robotics and Automation (ICRA)*, pp. 1–5, IEEE, 2018.

[16] C. R. Lee and C. T. Farley, "Determinants of the center of mass trajectory in human walking and running.," *Journal of experimental biology*, vol. 201, no. 21, pp. 2935–2944, 1998.

[17] W. Gao, Z. Jia, and C. Fu, "Increase the feasible step region of biped robots through active vertical flexion and extension motions," *Robotica*, vol. 35, no. 7, pp. 1541–1561, 2017.

[18] S. Caron, A. Escande, L. Lanari, and B. Mallein, "Capturability-based analysis, optimization and control of 3d bipedal walking," *arXiv preprint arXiv:1801.07022*, 2018.

Glossary

List of Acronyms

ICP	instantaneous capture point
CP	capture point
ZMP	zero moment point
CoP	center of pressure
CoM	center of mass
CMP	centroidal momentum pivot
LIP	linear inverted pendulum
2D	two-dimensional space
3D	three-dimensional space
MPC	model predictive control
GUI	graphical user interface
GRF	ground reaction force
SS	single support
DS	double support

List of Symbols

E_{LIP}	Linear inverted pendulum orbital energy
E_{LIP}	Linear inverted pendulum orbital energy
E_{orbit}	Nonlinear orbital energy
E_{orbit}	Nonlinear orbital energy
$_d$	Desired